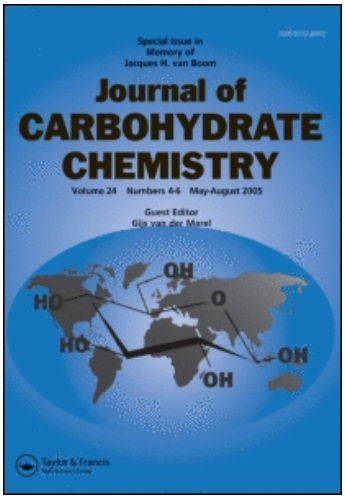

Journal of Carbohydrate Chemistry
Publication details, including instructions for authors and subscription information:
http://www.informaworld.com/smpp/title~content=t713617200

MM3 Modeling of Ribose and 2-Deoxyribose Ring Puckering

Michael K. Dowd; Alfred D. French; Peter J. Reilly

To cite this Article Dowd, Michael K. , French, Alfred D. and Reilly, Peter J.(2000) 'MM3 Modeling of Ribose and 2-Deoxyribose Ring Puckering', Journal of Carbohydrate Chemistry, 19: 9, 1091 — 1114
To link to this Article: DOI: 10.1080/07328300008544137
URL: http://dx.doi.org/10.1080/07328300008544137

J. CARBOHYDRATE CHEMISTRY, 19(9), 1091–1114 (2000)

MM3 MODELING OF RIBOSE AND 2-DEOXYRIBOSE RING PUCKERING

Michael K. Dowd,[a,*] Alfred D. French[a] and Peter J. Reilly[b]

[a]Southern Regional Research Center, U. S. Department of Agriculture, P. O. Box 19687, New Orleans, LA 70179, USA

[b]Department of Chemical Engineering, Iowa State University, Ames, IA 50011, USA

Received July 25, 2000 - Final Form September 21, 2000

ABSTRACT

Conformational energy maps for furanosyl and pyranosyl rings of α- and β-ribose and 2-deoxyribose were generated with the molecular mechanics program MM3. For the furanosyl tautomers, low-energy Northern and Southern minima were found. For the pyranosyl rings, lowest-energy minima corresponded to chair forms. Hydrogen-hydrogen coupling constants for the minimal-energy conformers were calculated based on Karplus equations. Computational and experimental results indicate that several tautomeric forms of ribose and 2-deoxyribose exist in multiple conformations in solution. Ring conformations of related crystal structures have energies within ~2 kcal/mol of the calculated global minima.

INTRODUCTION

Several research groups have recently attempted to understand the factors that affect the structures of nucleosides, nucleotides, and larger RNA and DNA fragments. Although the bases are relatively rigid, there is the possibility of conformational variation within the backbone and furanosyl ring components of nucleic acids. Crystallographic

studies show that ribofuranosyl and 2-deoxyribofuranosyl rings exist in two broadly defined conformational states,[1] and NMR studies of several RNA and DNA fragments indicate that significant amounts of these two conformational states exist in solution.[2-4] Recently, somewhat empirical attempts were made to understand the influence of the bases and the 3- and 5-exocyclic substituents on furanosyl ring conformations.[5-7] However, detailed conformational analysis has been lacking, in part hampered by a lack of understanding of the torsional energy of the C–O–C–N atom sequences that contain the anomeric centers in these compounds.[8]

Furanosyl rings are particularly challenging to model by classical mechanics methods. Unlike pyranosyl rings that typically have chair conformations, furanosyl rings have internal four-atom sequences that cannot all have *gauche* orientations that correspond to minima of the torsional components of the molecular potential function. Consequently, the balancing of relatively high-energy torsional effects contributes to the resulting low-energy structures, and accurate modeling requires that the torsional functions be correct over a range of -60° to +60° and not just in the regions corresponding to staggered conformations. In addition, the complex equilibria that generally exist for carbohydrates with furanosyl tautomers are often sensitive to temperature and solvent effects, which are difficult to model explicitly. Consequently, only a limited number of conformational studies have been conducted on the furanosyl sugars that form the backbone of nucleic acids.[9-16]

The molecular mechanics program MM3 has been used to study several furanosyl structures. Detailed studies have appeared for psicofuranose,[17] arabinofuranose,[18] and fructofuranose.[19] For the latter two compounds as well as for previously studied aldopyranosyl rings,[20] a large majority of accurately determined crystal conformations lies in low-energy regions within 2 kcal/mol of the MM3 global minimum, suggesting that reasonably accurate energy surfaces for ribose and 2-deoxyribose tautomers could be developed. Therefore, we extended our studies, based on the MM3 potential function, to include these compounds and have compared the results with crystallographic data. Results from NMR studies are also discussed. However, the modeling of NMR coupling constants and the prediction of tautomeric equilibria are generally less accurate for furanosyl rings than pyranosyl rings, largely due to the above-mentioned factors.

COMPUTATIONAL METHODS

In part to maintain continuity with our other studies on ring puckering, the 1992 version of MM3[21-23] was used in this work. Compared to the original 1990 code, this version has improved hydrogen bonding functionality and anomeric bond length corrections. The parameters associated with the hydrogen bonding functionality have been modified in newer version of the program; however, our studies on carbohydrate and inositol crystals (not yet published) suggest that the 1992 parameters better model these polyhydroxyl compounds. An elevated dielectric constant of 4.0 was used for all calculations, as this improves modeling of carbohydrates in condensed phases.[24] Conformational surfaces were generated with the block diagonal energy minimization method and the default termination criterion (0.08 cal/mol·atom).

The details of generating and maintaining puckered ring structures for optimization have been described elsewhere.[17,20] Briefly, sets of puckered structures were derived by moving two or three ring atoms and their associated attached atoms in the z direction perpendicular to an initial planar ring structure. The puckered shapes were maintained during minimization by fixing the z-coordinates of the ring atoms. For furanosyl rings, two non-adjacent ring atoms plus their non-ring substituents were moved in 0.1-Å increments over a range of -1 Å to +1 Å. This gives a total of 441 puckered ring forms. For each pyranosyl ring, three alternating ring atoms plus their substituents were moved in 0.1-Å increments from -0.8 Å to +0.8 Å, yielding 4913 ring forms. All combinations of staggered orientations of the exocyclic hydroxyl and hydroxymethyl groups were optimized for each puckered ring. Depending on the molecule and ring form, there were from three to five rotatable groups, yielding between 3^3 (=27) and 3^5 (=243) sets of starting structures. For each puckered ring, the lowest energy resulting from the different exocyclic starting structures was used to construct the conformational maps.

Ring puckering was quantified using the system of Cremer and Pople.[25] For furanosyl rings, the ring shape can be described with two parameters: a puckering amplitude (q) and a phase angle (ϕ). Conformational energy can be plotted as a function of these parameters in a plane-polar coordinate space. Fig. 1 shows the resulting furanosyl conformational space with the values of the Cremer-Pople phase angle and the locations of characteristic conformers. The puckering system of Altona and Sundaralingam is also

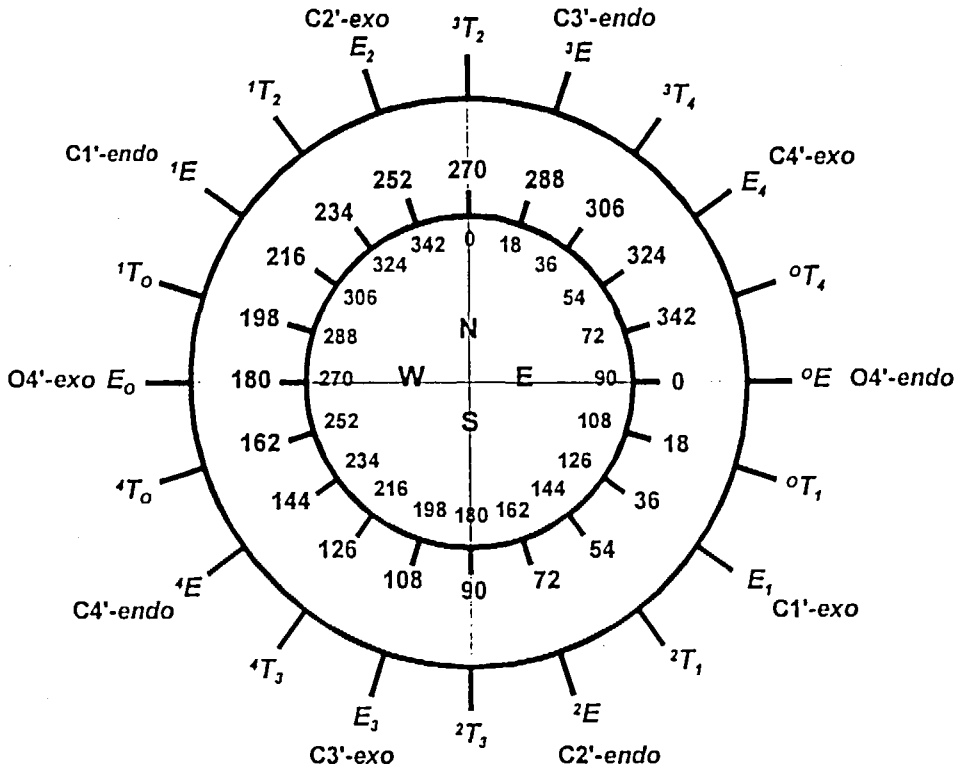

Figure 1. Representation of furanosyl ring puckering in polar conformational space. Phase angles are given for the puckering systems of Altona and Sundaralingham[26] (inner values) and Cremer and Pople[25] (outer values). Characteristic envelope and twist ring forms are denoted on the outer ring.

often used to describe the conformation of furanosyl rings,[26] so its phase angle (P) is shown, too. When divided by 100, the Altona-Sundaralingam puckering amplitude (generally denoted as τ_m, Φ_m, or χ_m) is equivalent to the Cremer-Pople puckering amplitude (q), and the phase angles differ by 90° ($\phi = P$ - 90°). For pyranosyl rings, three puckering parameters are required: a puckering amplitude (q), a phase angle (ϕ), and an inversion angle (θ). Although the pyranosyl parameters can be depicted in a spherical coordinate space, it is convenient to use the *plate carrée* (ϕ,θ) representation of Pickett and Strauss,[27] as the optimal puckering amplitude varies only from about 0.5 Å near the poles (chair forms) to 0.7 Å around the equator (skew and boat forms). This conform-

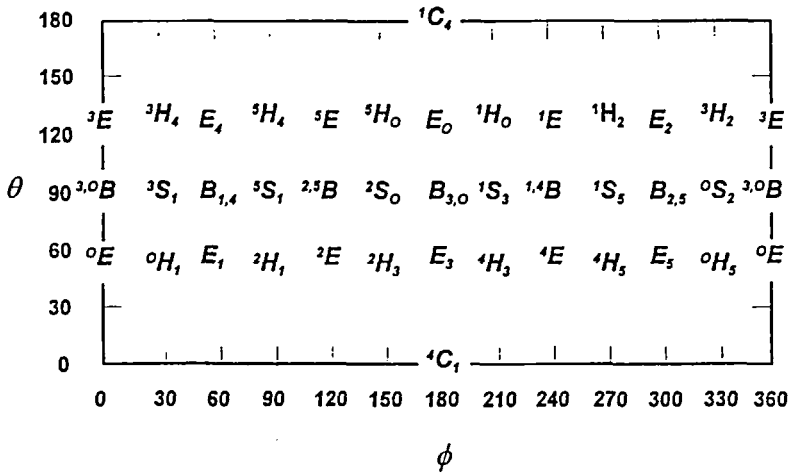

Figure 2. Pickett-Strauss surface (ϕ-θ) representing ribopyranosyl and 2-deoxyribopyranosyl ring shapes with the 38 characteristic chair, skew, boat, envelope, and half-chair forms denoted.

ational space is shown in Fig. 2 along with the locations of the characteristic chair, skew, boat, envelope, and half-chair ring forms. All conformational maps were generated using SURFER (Golden Software, Golden, CO) and annotated with DESIGNER (Micrografx, Richardson, TX).

After developing the conformational surfaces, local minima were determined by unrestrained optimization. The full matrix optimizer was used on the lowest-energy local grid-point structures from each of the low-energy regions of the maps. Hydrogen-hydrogen coupling constants were calculated for these structures with the Karplus equations of Haasnoot et al.[28] Where appropriate for furanosyl rings, corrections for Barfield transmission effects were included using the functions of de Leeuw et al.[29]

All structure generation and energy minimization calculations were completed with Project Vincent, a networked system of RISC-based DECstations at Iowa State University. Pentium-based microprocessors were used to calculate hydrogen-hydrogen coupling constants and puckering parameters for the minima and related crystal structures.

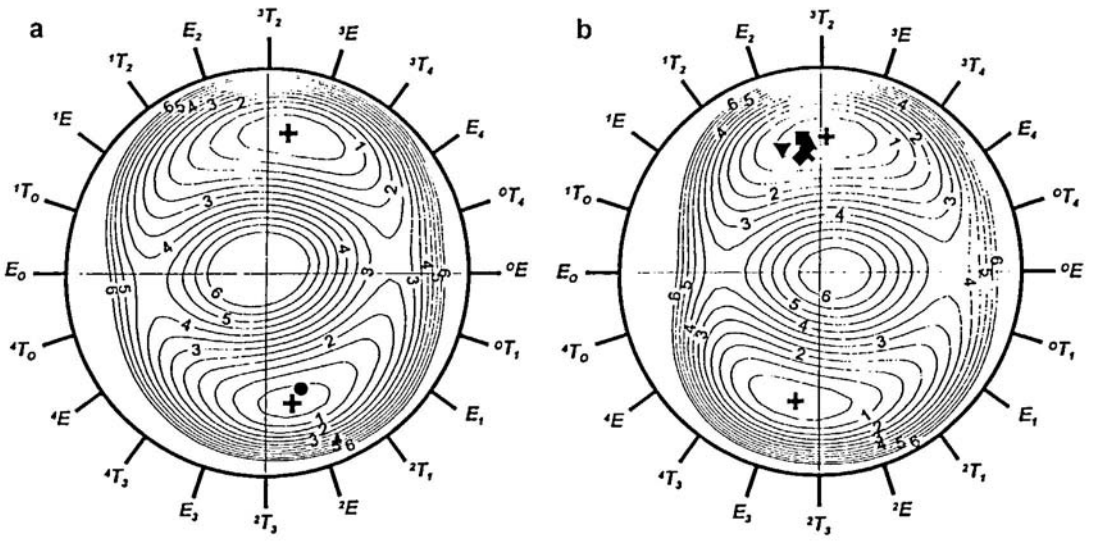

Figure 3. MM3(92)-generated ring puckering conformational maps for (a) α-ribofuranose and (b) β-ribofuranose with $\varepsilon = 4.0$. The outer circle corresponds to $q = 0.6$ Å. Energy contours are shown relative to the global minimum in increments of 0.5 kcal/mol. MM3 minima are denoted by (✚). The conformation of the ribofuranosyl ring in the barium α-ribofuranose-5-phosphate pentahemihydrate crystalline complex (●) is shown in (a).[26a] The conformations of the β-ribofuranosyl rings in the 1,2,3,5-tetra-*O*-acetyl-β-ribofuranoside crystal structures (▲, ◆),[27-29] the methyl β-ribofuranoside crystal structure (■, ▼),[13] and the 1-*O*-acetyl-2,3,5-tri-*O*-benozyl-β-ribofuranoside crystal structure (✕)[29a] are shown in (b).

RESULTS

Ribose. The conformational maps for α- and β-ribofuranose each show two broad low-energy regions (Fig. 3), with energies and puckering constants for their minima given in Table 1. The 1 kcal/mol energy contours of these regions extend over 40° to 50° of the ϕ puckering phase angle. Each map has one Northern minimum ($\phi \approx 270°$) and one Southern minimum ($\phi \approx 90°$), and their structures are shown in Fig. 4. Other furanosyl sugars have roughly similar maps.[17-19] For both ribose anomers, the global minimum is a Northern conformation, with the Southern minimum being only slightly greater in energy (0.09 and 0.15 kcal/mol). The α-anomer has a favored Eastern (through $\phi = 0°$) transitional pathway with a barrier of ~2.7 kcal/mol, while the β-anomer has almost equal Eastern and Western barriers of ~3.7 kcal/mol. The small energy differences, broad low-energy wells, and low energy barriers between the wells suggest that an equilibrium exists between Northern and Southern ring conformations in solution.

Table 1. MM3 energies and puckering parameters for ribose and 2-deoxyribose.

Tautomer	Conformer	MM3 energy[a] (kcal/mol)	q (Å)	ϕ (°)	θ (°)
Ribose					
α-Furanose	${}^3T_2/{}^3E$	12.38	0.417	278.21	
	${}^2E/{}^2T_3$	12.53	0.384	78.32	
β-Furanose	${}^3T_2$	10.53	0.394	273.64	
	${}^2T_3/E_3$	10.62	0.382	99.28	
α-Pyranose	${}^1C_4$	10.70	0.574	218.22	175.55
	${}^4C_1$	12.49	0.555	257.30	3.92
	${}^OS_2$	16.73	0.748	336.81	93.02
	${}^1S_3$	17.98	0.771	205.53	92.15
	${}^2S_O$	18.02	0.755	150.18	92.14
β-Pyranose	${}^4C_1$	10.84	0.584	15.26	3.07
	${}^1C_4$	11.07	0.536	76.88	175.90
	${}^2S_O$	13.78	0.756	152.59	88.72
	${}^3S_1$	16.01	0.762	23.60	87.75
	${}^1S_5$	19.00	0.715	273.39	86.07
2-Deoxyribose					
α-Furanose	${}^2E$	10.63	0.369	73.79	
	${}^3T_4$	11.35	0.410	306.86	
β-Furanose	${}^3T_2$	10.70	0.398	269.15	
	E_3	11.44	0.360	104.68	
α-Pyranose	${}^1C_4$	10.86	0.576	227.68	175.55
	${}^4C_1$	11.36	0.551	242.59	3.88
	${}^OS_2$	15.43	0.760	335.76	91.95
	${}^2S_O$	16.79	0.752	153.73	89.30
	${}^1S_3$	17.14	0.768	208.23	92.43
	${}^5S_1$	17.78	0.700	95.43	91.36
	${}^1S_5$	18.05	0.765	271.62	87.53
β-Pyranose	${}^1C_4$	10.06	0.544	26.05	177.82
	${}^4C_1$	11.14	0.582	355.44	3.91
	${}^3S_1$	15.21	0.768	23.60	88.15
	${}^2S_O$	15.29	0.749	152.68	88.91
	${}^1S_5$	16.97	0.739	271.91	86.87

a. Furanosyl ring energies have been corrected by -5.5 kcal/mol. This factor is part of MM3's heat of formation calculation but is not explicitly included in the steric energy. Its addition is necessary to make comparisons between pyranosyl and furanosyl ring forms.

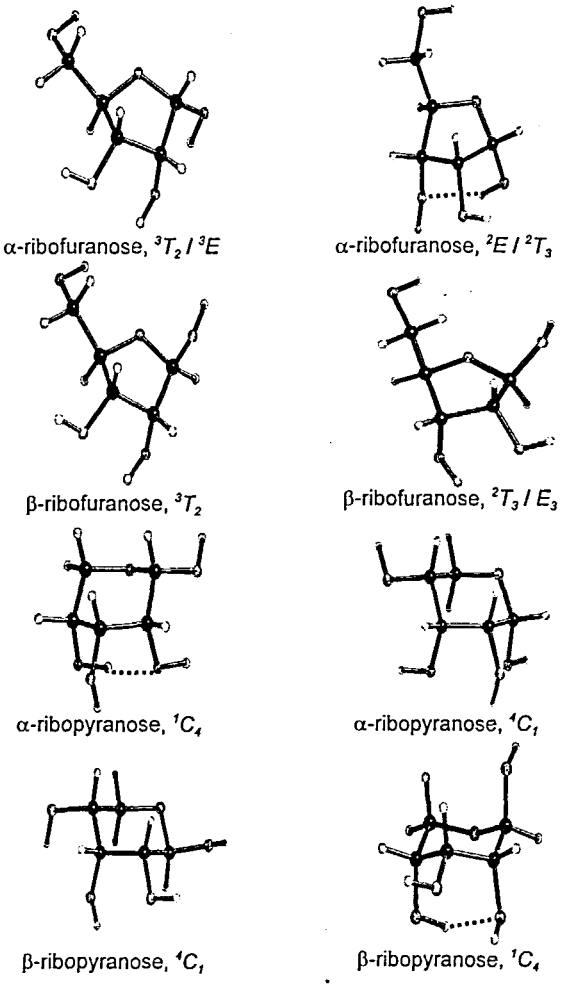

Figure 4. Structures at the global and secondary MM3 minima for the furanosyl and pyranosyl forms of ribose. For each tautomer, the global minimum is shown in the left column and the secondary mininum is shown in the right column. Intramolecular hydrogen bonds with oxygen-hydrogen distances < 2.1 Å are shown as dotted lines.

For α-ribofuranose, the Western transition barrier is significantly lower than for the previously studied α-ketosugars, all of which have a hydroxymethyl group attached to the anomeric carbon. This higher transition energy for the keto sugars is due to unfavorable steric interaction caused by the pseudo-axially-oriented hydroxymethyl groups at C-2 and C-5 for α-psicofuranose[17] and α-fructofuranose.[19] For β-ribofuranose, the Eastern transition barrier is lower in energy than for β-psicofuranose. The high transition energy of the latter sugar is due to an unfavorable eclipsing of the C-1–OH hydroxymethyl group at C-2 with the downward-oriented hydroxyl at C-3 in the ${}^{O}E$ conformation.[17] For β-fructofuranose, the Eastern transition barrier is similar to that of β-ribofuranose because the hydroxyl at C-3 is oriented upward and is not eclipsing the downward-oriented C-2 hydroxymethyl group.[19] Compared with the puckering amplitudes of the local minima (q = 0.38 to 0.42 Å), the transition-state conformers have smaller puckering amplitudes (q = ~0.29 Å), which indicates that some ring flattening occurs during pseudorotation.

The energy surface for β-ribopyranose suggests that both chair forms occur (Fig. 5). The difference in energy between these two forms is 0.23 kcal/mol, with the ${}^{4}C_{1}$ chair having the lower energy. For the α-anomer, the corresponding energy difference is 1.8 kcal/mol in favor of the ${}^{1}C_{4}$ form. Additional secondary minima corresponding to skew forms are also found on both maps. The energies of the skew conformers are high enough that they would not contribute significantly to the solution equilibrium.

2-Deoxyribose. As with ribose, the α- and β-2-deoxyribofuranose conformational maps each have large Northern and Southern low-energy regions (Fig. 6), with the 1 kcal/mol energy contours extending over 35° to 65° of the ϕ phase angle. For the α-anomer the global minimum is a Southern conformer (${}^{2}E$), while for the β-anomer the global minimum is a Northern conformer (${}^{3}T_{2}$) (Fig. 7). The energy differences between the global and second minima are about 0.7 kcal/mol for both anomers. Because there is an unfavorable eclipsing of the secondary hydroxyls at C-1 and C-2 in the ${}^{3}T_{4}$ conformation of α-ribofuranose that does not exist for 2-deoxy-α-ribofuranose, the locations of the Northern minima of the two forms are considerably different ($\Delta\phi$ = 29°). The β-anomers of the two furanoses do not exhibit a similar difference, due to the opposite orientation of the hydroxyl groups at C-1. As with α-ribofuranose, 2-deoxy-α-ribofuranose has a preferred Eastern pseudo-rotational pathway, but the energy barrier is only

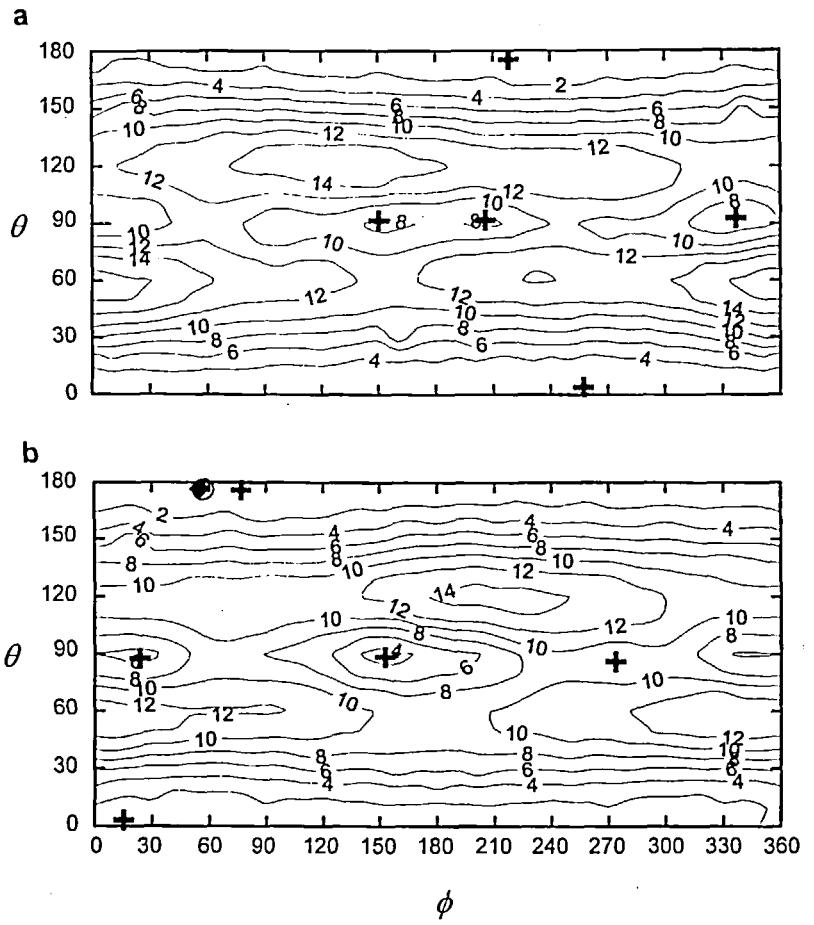

Figure 5. MM3(92)-generated Pickett-Strauss ϕ-θ conformational maps for α- and β-ribopyranose (a and b, respectively) with $\varepsilon = 4.0$. Energy contours are shown relative to the global minimum in increments of 2 kcal/mol up to 14 kcal/mol. Local minima are denoted by (✚). Crystallographic conformations for methyl β-ribopyranoside by x-ray and neutron diffraction[35,36] are illustrated by (○) and (◆), respectively.

~1.3 kcal/mol above the global minimal energy. The β-anomer has a slightly preferred Western transitional pathway with an energy barrier of ~2.2 kcal/mol. These transition-state energies for conversion between the two minima are lower for 2-deoxyribofuranose than for ribofuranose by 1.4 to 1.5 kcal/mol. The higher transitional energies for ribofuranose occur because of unfavorable eclipsing of its C-2 and C-3 vicinal hydroxyl groups in the transitional E_O or ${}^{O}E$ forms.

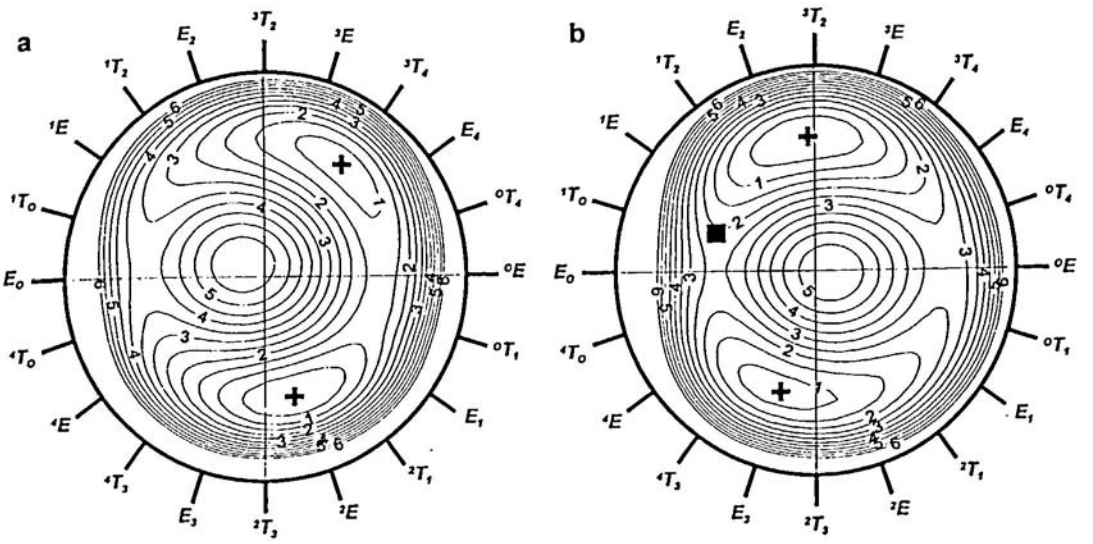

Figure 6. MM3(92)-generated ring puckering conformational maps for 2-deoxy-α- and 2-deoxy-β-ribofuranose (a and b, respectively) with $\varepsilon = 4.0$. The outer circle corresponds to $q = 0.6$ Å. Energy contours are shown relative to the global minimum in increments of 0.5 kcal/mol. Local minima are denoted by (✚). The crystallographic conformation of methyl 2-deoxy-3,5-di-*O*-*p*-nitrobenzoyl-β-ribofuranoside[37] is shown as (■).

Both 2-deoxyribopyranose anomers have lowest-energy regions corresponding to $^1C_4$ chairs (Fig. 8). The $^4C_1$ chairs are less stable by 0.5 and 1.1 kcal/mol for the α- and β-anomers, respectively. Local minima corresponding to skew forms also exist but are high in energy and, as seen for ribopyranose, are not likely to be major components of the solution equilibrium.

DISCUSSION

A few efforts to model ring shapes of ribose and 2-deoxyribose have appeared in the literature. Wiórkiewicz-Kuczera and Rabczenko studied methyl β-ribofuranose[12] and methyl 2-deoxy-β-ribofuranose[13] using the CFF molecular mechanics program of Melberg and Rasmussen.[39] A limited number of optimizations were considered, and curiously the methyl group was oriented *trans* to the O-4–C-1 bond, contrary to what would be expected based on the exo-anomeric effect. Using the same methodology, Tosi and Rasmussen[10] studied a 3,5-phospho-linked-diribofuranose structure. Levitt and

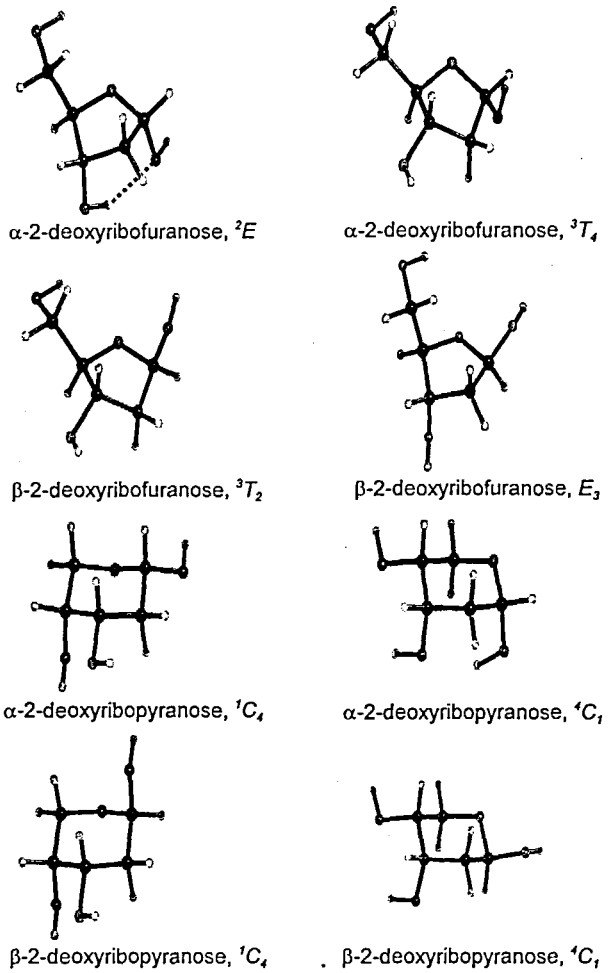

Figure 7. Structures at the global and secondary MM3 minima for the furanosyl and pyranosyl forms of 2-deoxyribose. For each tautomer, the global minimum is shown in the left column and the secondary mininum is shown in the right column. Intramolecular hydrogen bonds with oxygen-hydrogen distances < 2.1 Å are shown as dotted lines.

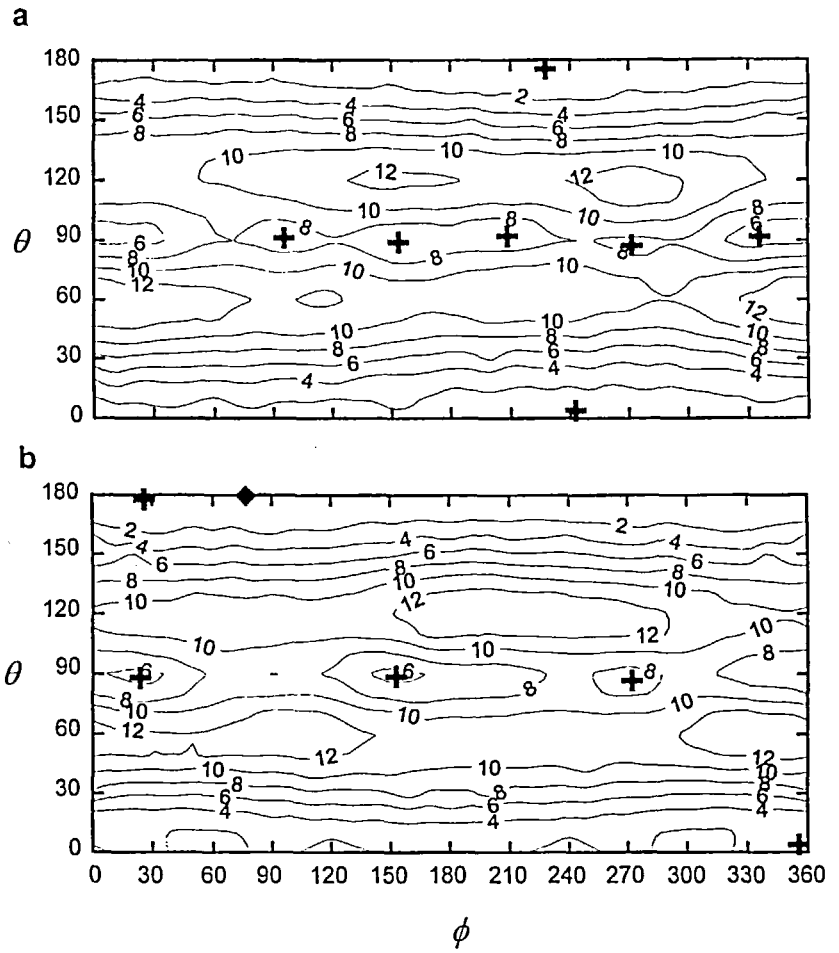

Figure 8. MM3(92)-generated ϕ-θ conformational surfaces for 2-deoxy-α- and 2-deoxy-β-ribopyranose (a and b, respectively) with $\varepsilon = 4.0$. Energy contours are shown relative to the global minimum in increments of 2 kcal/mol up to 14 kcal/mol. Local minima are denoted by (+). The crystallographic conformation of 2-deoxy-β-ribopyranose[38] is represented by (◆).

Warshel,[9] using their version of CFF, studied the 1-amino-1-deoxy derivatives of β-ribofuranose and 2-deoxy-β-ribofuranose, while Olson[11] studied 1-amino-1,5-dideoxy derivatives. Most recently, Gruza et al.[16] studied 5-deoxyribofuranose with the MM3 and AMBER potential functions. HF/6-31G* level ab initio calculations have been reported for the envelope forms of methyl-β-ribofuranose[14] and methyl-β-2-deoxyribofuranose.[15]

Table 2. Experimental and calculated distributions of ribose and 2-deoxyribose tautomers.

Pyranose		Furanose		Conditions	Reference
α	β	α	β		
Ribose					
18	54	12	16	70 °C, D_2O	40
21.5	58.5	6.5	13.5	31 °C, D_2O	41
20.3	62	6.1	11.6	30 °C, D_2O	42
19	64	6	11	30 °C, D_2O	43
23	55	8	14	30 °C, D_2O	44
16	54	6	24	35 °C, DMSO-d_6	44
20-23	54-62	6.1-8.8	11-15	21-48 °C, D_2O, pH 4.8-7.0	45
21	27	2	50	MM3	
2-Deoxyribose					
39-41	37.5-40.5	10-12	8.6-10.5	21-36 °C, D_2O, pH 4.5-7.0	45
15	47	20	18	MM3	

Most of these computational studies suggest that both Northern and Southern conformers exist in significant amounts for these compounds. Relative energies of the various minima differ as do the transitional energy barriers between the minima. These differences likely result from the different computational methods used and the different structures studied.

The distributions of ribosyl tautomers have been determined in different environments using NMR methods (Table 2).[40-45] All reports indicate that the β-pyranosyl form is the most prevalent and the α-furanosyl form the least. The distribution based on the MM3 steric energies suggests that the α-furanosyl form is the least prevalent but overestimates the amount of the β-furanosyl form and underestimates that of the β-pyranosyl form. For 2-deoxyribose, experiment indicates that more of the α-pyranosyl form and less of the other three forms are present than is found by MM3.[45] Because of the narrow range of energies calculated for the various forms, the calculated equilibria of these sugars are sensitive to modeling errors and to the lack of accounting for explicit solvent interactions. Inclusion of entropic components from the MM3-calculated vibrational spectra did not significantly improve the comparison.

Angyal has discussed the effect of substituents on the distribution of the various tautomeric forms.[46] He proposed that more of the furanosyl forms exist for deoxyaldoses than for the corresponding aldoses due to reduced eclipsing interactions between adjacent hydroxyl groups. This is not found experimentally for ribose and 2-deoxyribose, with about equal amounts of two furanosyl forms found for both compounds (Table 2). MM3 has not reproduced this effect either, with 52% furanosyl form calculated for ribose and 38% for 2-deoxyribose. Angyal[46] also proposed that 2-deoxyfuranosyl sugars would contain roughly equal amounts of the α- and β-anomeric forms due to the lack of prohibitive eclipsing of hydroxyl groups. For 2-deoxyribofuranose, the equilibrium contains roughly equal amounts of the α- and β-anomers by experiment and by MM3. For ribofuranose, more of the β-anomer is expected because of the downward orientation of the C-2 hydroxyl and eclipsing of the O-1 when it is in the α-configuration. This is reflected by experiment and by MM3.

Crystal structures have been reported for several compounds containing a ribofuranosyl ring. The barium α-ribofuranose-5-phosphate complex has been studied by Koziol and Lis.[30] This furanosyl ring has a Southern conformation (q = 0.342 Å, ϕ = 73.8°) and lies close to the 0.5 kcal/mol MM3 energy contour (Fig. 3a). Crystal structures have also been reported for methyl β-ribofuranoside,[14] 1,2,3,5-tetra-*O*-acetyl-β-ribofuranose,[31-33] and 1-*O*-acetyl-2,3,5-tri-*O*-benzyl-β-ribofuranose.[34] All of these β-furanosyl structures have similar $^3T_2$ Northern conformations and lie within the 0.5 kcal/mol contour line of the MM3 global low-energy region (Fig. 3b).

X-ray and neutron diffraction structure determinations have been carried out for methyl β-ribopyranoside.[35,36] This structure has a $^1C_4$ conformation and lies within the second low-energy region of the β-ribopyranose map, within 0.3 kcal/mol of the lowest energy conformer (Fig. 5b).

One crystal structure containing a 2-deoxyribofuranosyl ring, methyl 2-deoxy-3,5-di-*O*-*p*-nitrobenzoyl-β-ribofuranoside, has been reported.[37] Its ring lies within the global low-energy well of the β-ribofuranosyl map but along the surface gradient corresponding to the favored Western transitional pathway at the ~2 kcal/mol contour (Fig. 6b). Because this conformation is near a transitional point on the β-ribofuranosyl energy map, it was of interest to understand whether the large *p*-nitrobenzoyl substituents, crystal packing effects, or a combination of the two factors affected the ring conformation. To

estimate the influence of the bulky benzoyl substituents, two di-*O*-benzoylfuranoside derivative structures were MM3-optimized. One optimization was started from the crystallographic conformation, while the other was started from the MM3 global low-energy conformation of the unsubstituted β-2-deoxyribofuranose ring. In these optimizations, the nitro moieties were removed, as torsional and valence angle constants are lacking for the original compound. Because the replaced ligands are at isolated ends of the molecule, the substitutions should not greatly influence the ring conformation during optimization. Energy minimization from the crystallographic conformation shifted the ring conformation from a ${}^{1}T_{O}$ form to an $E_2/{}^{3}T_2$ form (q = 0.390 Å, ϕ = 259°). This ring conformation is close to the 2-deoxyribofuranose global minimum within the 0.5 kcal/mol contour. Energy minimization from the global minimum conformation yielded a similar $E_2/{}^{3}T_2$ form (q = 0.391 Å, ϕ = 257°). These results suggest that crystal packing is responsible for most of the unusual puckering of the ring.

The crystal structure of 2-deoxy-β-ribopyranose[38] has a ${}^{1}C_{4}$ conformation. This conformation lies in the MM3 calculated global low-energy region (Fig. 8b).

Numerous crystal structures have been reported for ribo- and 2-deoxyribofuranosyl nucleosides and nucleotides, and the conformations of these structures have been reviewed and discussed in detail.[1] The furanosyl rings of these compounds tend to have either Northern and Southern conformations. Crystals with Northern conformations generally lie between the ${}^{3}T_2$ and ${}^{3}T_4$ regions of the map (270° < ϕ < 306°) but with a few ribofuranosyl structures extending to the E_2 form (ϕ ~ 244°). The Southern conformations generally fall between the ${}^{2}T_1$ and ${}^{2}T_3$ map regions (54° < ϕ < 90°) but with a few structures extending to the ${}^{4}T_3$ conformation (ϕ ~ 126°). All of these crystallographic ring structures lie within the 2 kcal/mol contours of the corresponding MM3 furanosyl maps, although as a group the conformations are shifted away from the centers of the low-energy wells toward the Eastern regions of the maps. Unfortunately, only preliminary studies have been undertaken to parameterize the C–O–C–N torsional sequences contained by these compounds.[8] A more detailed conformational analysis of the influence of the nitrogenous base on the ring structure is dependent upon accurate parameterization of this torsional sequence.

Two 2-deoxyribopyranosyl nucleoside compounds have been studied by x-ray crystallography.[47,48] As was the case with 2-deoxyribopyranose, these rings have ${}^{1}C_{4}$

conformations that lie within the global low-energy well of the 2-deoxyribopyranosyl energy map.

Hydrogen-hydrogen coupling constants have been reported for methyl α-ribofuranoside,[49] methyl β-ribofuranoside,[49,50] α- and β-ribopyranose,[51] methyl α- and β-ribopyranoside,[51] α-methyl-2-deoxyribofuranoside[50,52] and β-methyl-2-deoxyribofuranoside.[15,50,52] Coupling constants calculated for the individual low-energy MM3 minima and average coupling constants based on the MM3 energies are given in Tables 3 and 4. Because structures can be easier to predict than energies, the distributions of conformers and the average coupling constants were also determined by a least-squares best fit of the individual coupling constants determined for each of the important low-energy minima with the experimental data.

Coupling constants for methyl α-ribofuranoside were reported by Kline and Serianni.[49] Their analysis, based on $^3J_{H,H}$, $^3J_{C,H}$ and $^3J_{C,C}$ data, suggests a preference for the a Southern conformer between the E_1 and ^2E forms. The coupling constants calculated from the MM3 local minima suggest that a distribution of Northern and Southern conformers exist, although the J_{23} value (Table 3) is especially problematic because it is higher in value than the J_{23} value of both MM3 local minima. The MM3 energy values indicate a slight preference for the Northern region (0.56 $^3T_2/^3E$). The root-mean-squared (RMS) deviation between the modeled and experimental coupling constants is 1.4 Hz, which is greater than the reported standard error of ~0.4 Hz associated with the Karplus model.[28] A best-fit model shifts the distribution toward the Southern form (0.36 $^3T_2/^3E$) and reduces the RMS deviation to 1.1 Hz, most of which is contributed by the discrepancy in J_{23}. The high value of this coupling constant is suggestive of structures shifted toward the Western side of the conformational space, consistent with the proposed E_1 to ^2E structure. In this regard, the representation of the large low-energy conformational regions exhibited by these molecules as a single conformer may be an over simplification that contributes significantly to deviations between the calculated and experimental result. On this point, Cros et al.[18] have shown that the variation in the values of some ring coupling constants can be large over the low-energy areas that are typically exhibited on furanosyl puckering maps. Hence, representing these broad regions by a single conformation may not be an adequate model for these compounds.

For methyl β-ribofuranoside, similar coupling constants were reported by Kline and Serianni[49] and Gerlt and Youngblood.[50] Both data sets suggest that some distribution

Table 3. Calculated and experimental hydrogen-hydrogen coupling constants for ribose.[a]

Conformer	J_{12}	J_{23}	J_{34}	J_{45u}	J_{45d}	RMS dev.	Ref.
α-Furanose							
$^3T_2/^3E$	3.2	4.3	8.8				
$^2E/^2T_3$	4.6	4.6	0.7				
MM3 ave. (0.56 $^3T_2/^3E$)	3.9	4.4	5.0			1.4	
Best fit (0.36 $^3T_2/^3E$)	4.1	4.4	3.6			1.1	
Exp.[b]	4.3	6.2	3.4				49
β-Furanose							
$^3T_2$	0.3	4.5	8.4				
$^2T_3/E_3$	3.8	4.8	0.7				
MM3 ave. (0.51 $^3T_2$)	2.0	4.6	4.7			1.2[c]	
Best fit[c] (0.77 $^3T_2$)	1.1	4.6	6.6			0.2	
Exp.[d]	1.2	4.6	6.9				49
Exp.[d]	0.8	4.7	6.5				50
α-Pyranose							
$^1C_4$	1.2	2.7	3.0	1.1	2.7		
$^4C_1$	3.5	3.0	2.8	5.7	10.6		
MM3 ave. (0.95 $^1C_4$)	1.3	2.7	3.0	1.3	2.7	1.0[e]	
Best fit[e] (0.64 $^1C_4$)	2.0	2.8	2.9	2.7	5.2	0.1	
Exp.[f]	2.1	3.0	3.0	2.6	5.3		51
Exp.[g]	3.0	3.2	3.2				51
β-Pyranose							
$^4C_1$	7.2	2.9	2.7	5.8	10.6		
$^1C_4$	2.3	3.0	2.8.	1.0	2.4		
MM3 ave. (0.60 $^4C_1$)	5.2	2.9	2.7	3.9	7.3	1.0[h]	
Best fit[h] (0.78 $^4C_1$)	6.1	2.9	2.7	4.7	8.8	0.3	
Exp.[i]	6.5	3.3	3.2	4.4	8.8		51
Exp.[j]	5.1	3.4	3.4	3.5	7.0		51

a. Calculated from the Karplus equations of Haasnoot et al.[28] with corrections for the cisoidal hydrogen pairs of furanosyl rings calculated as described by de Leeuw et al.[29] b. Methyl α-ribofuranose in D_2O. c. Based on the data from Gerlt and Youngblood.[50] d. Methyl β-ribofuranoside in D_2O. e. Based on data for α-ribopyranose.[51] f. α-Ribopyanose in D_2O. g. Methyl α-ribopyranoside in D_2O. h. Based on the data for β-ribopyranose.[51] i. β-Ribopyanose in D_2O. j. Methyl β-ribopyranoside in D_2O.

Table 4. Calculated and experimental hydrogen-hydrogen coupling constants for 2-deoxyribose.[a]

Conformer	J_{12u}	J_{12d}	J_{2u3}	J_{2d3}	J_{34}	J_{45u}	J_{45d}	RMS dev.	Ref.
α-Furanose									
^2E	4.9	1.3	4.6	1.5	0.9				
$^3T_4$	6.6	5.9	7.9	9.0	8.6				
MM3 ave. (0.77 ^2E)	5.3	2.4	5.5	3.6	3.2			1.0[b]	
Best fit[b] (0.71 ^2E)	5.4	2.6	5.5	3.6	3.2			1.0	
Exp[c]	5.3-5.4	1.0-1.7	7.3-7.5	2.3-3.1	3.4-3.9				52
Exp[d]	5.0	0.9	7.2	2.2	2.7				52
β-Furanose									
$^3T_2$	1.2	4.7	7.0	10.1	7.8				
E_3	7.8	6.2	4.9	1.4	0.8				
MM3 ave. (0.78 $^3T_2$)	2.7	5.6	6.5	8.2	6.3			1.3[e]	
Best fit[e] (0.59 $^3T_2$)	4.0	5.3	6.1	6.4	4.9			0.8	
Exp.[f]	2.6	5.4	6.7	~5.7	4.2				15
Exp.[f]	2.5	5.8	6.6	6.2	4.1				50
Exp.[f]	2.7	5.5	6.7	5.9	4.2				52
Exp.[g]	2.0	5.7	6.8	5.8	3.8				52
α-Pyranose									
$^1C_4$	3.3	10.6	4.9	11.1	2.9	1.0	2.4		
$^4C_1$	3.9	2.2	2.5	3.6	2.7	5.8	10.6		
MM3 ave. (0.70 $^1C_4$)	3.5	8.1	4.2	8.8	2.8	2.4	4.9		
β-Pyranose									
$^1C_4$	2.3	3.7	4.9	11.0	2.7	1.0	2.4		
$^4C_1$	10.5	3.5	2.5	3.5	2.9	5.8	10.6		
MM3 ave. (0.86 $^1C_4$)	3.4	3.7	4.6	10.0	2.7	1.7	3.5		

a. Calculated values are from the Karplus equations of Haasnoot et al.[28] with corrections for cisoidal hydrogen pairs within furanosyl rings made as described by de Leeuw et al.[29] b. Based on data for methyl 2-deoxy-α-ribofuranoside in D_2O at 292 K.[52] c. Methyl 2-deoxy-α-ribofuranoside in D_2O between 271 and 346 K. d. Methyl 2-deoxy-α-ribofuranoside in $CDCl_3$. e. Based on data for methyl 2-deoxy-β-ribofuranoside in D_2O.[52] f. Methyl 2-deoxy-β-ribofuranoside in D_2O. g. Methyl 2-deoxy-β-ribofuranoside in $CDCl_3$.

of Northern and Southern conformers exists. Based on the MM3 energies for the free sugars, the Northern form is predicted to be slightly favored (51%) over the Southern form. The RMS deviation between the modeled and experimental coupling constants is 1.2 Hz. The best fit procedure results in a somewhat greater concentration of the Northern form (77%) and with a significantly smaller RMS deviation of the fitted results (0.2 Hz). The conformer energy difference necessary to yield this distribution is 0.71 kcal/mol.

For α-ribopyranose, the experimental coupling constants suggest that both chairs exist in solution. Based on MM3 steric energies, the distribution is >95% $^1C_4$ and the RMS deviation of the calculated and experimental coupling constants is 1.0 Hz. A least-squares fitting of the coupling constants yields a distribution that is 64% $^1C_4$ (0.34 kcal/mol conformer energy difference) with an RMS deviation of 0.1 Hz. For β-ribopyranose, the MM3-predicted distributions are closer, with 60% $^4C_1$ predicted by the MM3 energies and 78% (0.75 kcal/mol conformer energy difference) predicted by the least squares fitting of individual chair coupling constants to the experimental data. Franks et al.[44] reported a $^4C_1/^1C_4$ ratio of β-ribopyranose of 74:26 at 30 °C in D_2O. From their report, it is clear that this ratio is somewhat sensitive to temperature and solvent changes. For both anomeric forms, the RMS deviations between experimental and calculated values are significantly reduced by the least-squares fitting of the coupling constants. For pyranosyl rings that are known to exist as chairs, this suggests predicted chair energies are in error.

Raap et al.[52] discussed the conformations of methyl α- and methyl β-2-deoxy-ribofuranosides based on fitting coupling constant data recorded for several solvent conditions. Church et al.[15] has recently reported comparable data and analysis for methyl β-2-deoxy-ribofuranoside. In the former report, the coupling constants of each anomer were best reproduced with a two-conformer model consisting of one Northern and one Southern conformer. For the α-anomeric form, the percentage of the Southern form in D_2O increased from 79 to 94% as the temperature decreased from 346 K to 271 K, which indicates that there is a significant entropy difference between the two forms. For the β-anomer, the conformer distribution was 61% Northern in D_2O, and the results were not sensitive to temperature. In comparison, the conformer distribution based on the MM3 energies for the α-anomer of 2-deoxyribofuranose is 77% Southern.

Using a best-fit criterion, the distribution predicted is 71% Southern (0.53 kcal/mol conformer energy difference). For the β-anomer, the conformer distribution is 78% Northern based on the MM3 energies, while a best-fit criterion yields a 59% Northern distribution (0.21 kcal/mol conformer energy difference). The RMS deviations between the experimental data and the MM3 results improved only modestly by the least squares fitting of the minimal distribution. Although the coupling constant differences are less than those derived using the CFF potential by Wiórkiewicz-Kuczera and Rabczenko,[13] the deviations are larger than the 0.3 to 0.5 Hz obtained by Rapp et al.[52] The lack of improvement in the deviation when the MM3 energies were ignored and the distribution was predicted by fitting suggests that a component of the error is associated with the individual structures used to represent the Northern and Southern low-energy regions. The differences between the modeled deviations produced by MM3 and the Rapp et al. model stem from the same effect, as the conformations of the local minima derived from the two approaches are different. This is apparent in the different phase angles for the various conformers. For methyl α-2-deoxyribofuranoside, the Southern conformer derived by Rapp et al. has a Cremer-Pople ϕ value of ~42° compared with the 74° value found by MM3 for the free sugar. For the β-form, both of the Rapp et al. conformers are located toward the Western side of the map relative to the MM3 results, with the Northern minimum lying near $\phi = 245°$ and the Southern minimum lying near $\phi = 144°$. Although the Rapp et al. fitting method yields a low RMS deviation from the experimental results, their procedure is very sensitive to any errors in the experimental values, and it is possible for a wide range of puckering parameters to be encompassed within this error, i.e., a small deviation in the experimental coupling constants can result in a large change in the predicted conformations. One consequence of the different derived phase angles is that the NMR-based study suggests a clear difference between the predicted ring conformations of the methyl 2-deoxyribofuranosides and the ring conformations of crystalline 2-deoxyribonucleosides and nucleotides. The MM3-derived structures diverge less from the crystallographic results.

The full-matrix optimization method available within MM3 permits calculation of the vibrational spectra and the entropies for freely optimized structures. These calculations can be conducted only for structures derived from fully unconstrained optimizations. Hence, they are not applicable to typical applications of conformational analysis,

such as our development of energy surfaces for ring puckering. In general, the resulting MM3-derived free energies from these calculations have not systematically changed the gross distribution of carbohydrate conformational or anomeric forms, and we have often effectively assumed that the entropies of these local structures are identical. This was intended as an initial treatment until it can be established that the errors in the computed vibrations are small for hydroxyl-containing compounds and that including these effects improves comparisons with experimental data. These calculations were explicitly included and discussed in our study of the inositol rings,[53] because it is generally assumed that entropic effects lower the free energy of *myo*-inositol below the free energy of *scyllo*-inositol. In that work, MM3 predicted that the entropy of the *myo* form was higher than that for the *scyllo* form, although not to the extent that the free energy was lower for *myo*-inositol at 298 K.[53] For all but one of the compounds considered in the present work, the effect of including entropic effects based on the MM3-predicted vibrational spectra was relatively small. The exception was for 2-deoxy-α-ribofuranose. For this compound, the computed entropy was higher for the Northern form by ~2.6 eu. Higher entropy of the Northern form agrees with the temperature-dependent NMR results of Rapp et al.[52] on the methyl derivative, although the magnitude of the entropic difference estimated by MM3 is larger than the temperature-induced changes warrant. Including the entropic factors, the MM3 calculations yield a conformer distribution slightly favoring the Northern form (58%) at 298 K, which is not supported by the NMR results.

CONCLUSIONS

MM3 modeling for ribose and 2-deoxyribose suggests that each molecule exists in a complicated equilibrium of tautomeric and conformational forms. The discrepancies between our calculated energies and the apparent free energies derived from NMR results were less than 1.0 kcal/mol, very good for a modeling exercise. Unfortunately, discrepancies of this magnitude are large enough that tautomer and conformer equilibria are not very accurately predicted.

Ring conformations in related crystals were within 2 kcal/mol of the MM3-predicted low-energy structures. Ribo- and 2-deoxyribonucleoside and nucleotide crystal structures also fall within this energy range, although both Northern and Southern ring

conformations appear to be located toward the Western side of the MM3-derived low-energy regions. Although there are differences in the solution populations predicted by using molecular mechanics energies and those achieved exclusively by fitting NMR coupling constants, the results are qualitatively similar. Both approaches suggest that populations of Northern and Southern minima are present for ribofuranose and 2-deoxy-ribofuranose, and that the distribution of the α-form of the latter compound is shifted more toward the Southern form.

REFERENCES

1. H. P. M. de Leeuw, C. A. G. Haasnoot, and C. Altona, *Isr. J. Chem.*, **20**, 108 (1980).
2. C. A. G. Haasnoot, F. A. A. M. de Leeuw, H. P. M. de Leeuw, and C. Altona, *Org. Magn. Reson.*, **15**, 43 (1981).
3. A. J. Hartel, G. Wille-Hazelager, J. H. van Boom, and C. Altona, *Nucleic Acids Res.*, **9**, 1405 (1981).
4. J. -R. Mellema, C. A. G. Haasnoot, J. H. van Boom, and C. Altona, *Biochim. Biophys. Acta*, **655**, 256 (1981).
5. C. Thibaudeau, J. Plavec, N. Garg, A. Papchikhin, and J. Chattopadhyaya, *J. Am. Chem. Soc.*, **116**, 4038 (1994).
6. J. Plavec, C. Thibaudeau, and J. Chattopadhyaya, *J. Am. Chem. Soc.*, **116**, 6558 (1994).
7. J. Plavec, C. Thibaudeau, and J. Chattopadhyaya, *J. Am. Chem. Soc.*, **116**, 8033 (1994).
8. R. K. Jalluri, Y. H. Yuh, and E. W. Taylor, *ACS Symp. Ser.* **539**, 277 (1993).
9. M. Levitt and A. Warshel, *J. Am. Chem. Soc.*, **100**, 2607 (1978).
10. C. Tosi and K. Rasmussen, *Biopolymers*, **20**, 1059 (1981).
11. W. K. Olson, *J. Am. Chem. Soc.*, **104**, 278 (1982).
12. J. Wiórkiewicz-Kuczera and A. Rabczenko, *J. Chem. Soc., Perkin Trans. 2*, 789 (1985).
13. J. Wiórkiewicz-Kuczera and A. Rabczęnko, *J. Chem. Soc., Perkin Trans. 2*, 437 (1986).
14. C. A. Podlasek, W. A. Stripe, I. Carmichael, M. Shang, B. Basu, and A. S. Serianni, *J. Am. Chem. Soc.*, **118**, 1413 (1996).
15. T. J. Church, I. Carmichael, and A. S. Serianni, *J. Am. Chem. Soc.*, **119**, 8946 (1997).
16. J. Grůza, J. Koča, S. Pérez, and A. Imberty, *J. Mol. Struct. (Theochem)*, **424**, 269 (1998).
17. A. D. French and M. K. Dowd, *J. Comput. Chem.*, **15**, 561 (1994).
18. S. Cros, C. Hervé du Penhoat, S. Pérez, and A. Imberty, *Carbohydr. Res.*, **248**, 81 (1993).
19. A. D. French, M. K. Dowd, and P. J. Reilly, *J. Mol. Struct. (Theochem)*, **395-396**, 271 (1997).
20. M. K. Dowd, A. D. French, and P. J. Reilly, *Carbohydr. Res.*, **264**, 1 (1994).
21. N. L. Allinger, Y. H. Yuh, and J. H. Lii, *J. Am. Chem. Soc.*, **111**, 8551 (1989).

22. J. H. Lii and N. L. Allinger, *J. Am. Chem. Soc.*, **111**, 8566 (1989).
23. N. L. Allinger, M. Rahman, and J. H. Lii, *J. Am. Chem. Soc.*, **112**, 8293 (1990).
24. A. D. French and M. K. Dowd, *J. Mol. Struct. (Theochem)*, **286**, 183 (1993).
25. D. Cremer and J. A. Pople, *J. Am. Chem. Soc.*, **97**, 1354 (1975).
26. C. Altona and M. Sundaralingam, *J. Am. Chem. Soc.*, **94**, 8205 (1972).
27. H. M. Pickett and H. L. Strauss, *J. Am. Chem. Soc.*, **92**, 7281 (1970).
28. C. A. G. Haasnoot, F. A. A. M. de Leeuw, and C. Altona, *Tetrahedron*, **36**, 2783 (1980).
29. F. A. A. M. de Leeuw, A. A. van Beuzekom, and C. Altona, *J. Comput. Chem.*, **4**, 438 (1983).
30. A. E. Koziol and T. Lis, *Acta Crystallogr., Sect. C*, **47**, 2076 (1991).
31. V. J. James and J. D. Stevens, *Cryst. Struct. Commun.*, **2**, 609 (1973).
32. B. J. Poppleton, *Acta Crystallogr., Sect. B*, **32**, 2702 (1976).
33. M. Czugler, A. Kálmán, J. Kovács, and I. Pintér, *Acta Crystallogr., Sect. B*, **37**, 172 (1981).
34. R. Kingsford-Adaboh and S. Kashino, *Bull. Chem. Soc. Jpn.*, **65**, 3477 (1992).
35. V. J. James and J. D. Stevens, *Carbohydr. Res.*, **21**, 334 (1972).
36. V. J. James, J. D. Stevens, and F. H. Moore, *Acta Crystallogr., Sect. B*, **34**, 188 (1978).
37. J. Raap, J. H. van Boom, H. J. Bruins Slot, P. T. Beurskens, J. A. C. van Wietmarschen, J. M. M. Smits, and C. A. G. Haasnoot, *Acta Crystallogr., Sect. B*, **43**, 219 (1987).
38. S. Furberg, *Acta Chem. Scand.*, **14**, 1357 (1960).
39. S. Melberg and K. Rassmussen, *J. Mol. Struct.*, **57**, 215 (1979).
40. M. Rudrum and D. F. Shaw, *J. Chem. Soc.* 52 (1965).
41. S. J. Angyal and V. A. Pickles, *Aust. J. Chem.*, **25**, 1695 (1972).
42. E. Breitmaier and U. Hollstein, *Org. Magn. Reson.*, 8, **573** (1976).
43. D. Horton and Z. Walaszek, *Carbohydr. Res.*, **105**, 145 (1982).
44. F. Franks, P. J. Lillford, and G. Robinson, *J. Chem. Soc., Faraday Trans. 1*, **85**, 2417 (1989).
45. S. J. Cortes, T. L. Mega, and R. L Van Etten, *J. Org. Chem.*, **56**, 943 (1991).
46. S. J. Angyal, *Adv. Carbohydr. Chem. Biochem.*, **42**, 15 (1984).
47. P. D. Robinson, C. Y. Meyers, V. M. Kolb, and P. A. Colloton, *Acta Crystallogr., Sect. C*, **52**, 1215 (1996).
48. V. M. Kolb, P. A. Colloton, P. D. Robinson, H. G. Lutft, and C. Y. Meyers, *Acta Crystallogr., Sect. C*, **52**, 1781 (1996).
49. P. C. Kline and A. S. Serianni, *J. Am. Chem. Soc.*, **112**, 7373 (1990).
50. J. A. Gerlt and A. V. Youngblood, *J. Am. Chem. Soc.*, **102**, 7433 (1980).
51. K. Bock and H. Thøgersen, *Ann. Rep. NMR Spectrosc.*, **13**, 1 (1982).
52. J. Raap, J. H. van Boom, H. C. van Lieshout, and C. A. G. Haasnoot, *J. Am. Chem. Soc.*, **110**, 2736 (1988).
53. M. K. Dowd, A. D. French, and P. J. Reilly, *Aust. J. Chem.*, **49**, 327 (1996).